Thermo X
https://doi.org/10.70401/tx.2026.0031

Supplementary information

Insights into lattice thermal transport mechanisms in layered chalcogenides X_2PdY_6 (X = Nb, Ta; Y = S, Se) via machine learning molecular dynamics simulations

Xiguang Wu, Jianlian Huang, Weikuan Li, Yuxuan Guo, Wei Zhang, Yajuan Cheng, Gang Zhang, Shiyun Xiong

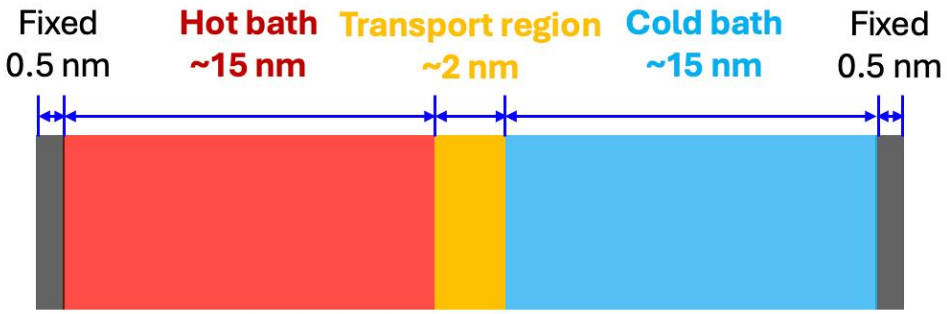

Figure S1. Schematic setup for NEMD simulations.

The NEMD simulation setup is schematically illustrated in Fig. S1. The two terminal regions, each with a length of 0.5 nm, were fixed. The heat-source and heat-sink regions had lengths of 15.0 nm. The spectral heat current was evaluated in the central transport region, whose length was ~ 2 nm. Periodic boundary conditions were applied along transverse directions.

Each system was equilibrated for 200 ps in the NPT ensemble and subsequently for 200 ps in the NVT ensemble, using a 1 fs time step. An NEMD simulation was then performed for 1 ns using Langevin heat baths to build the non-equilibrium steady state. Subsequently, another 1 ns of NEMD simulation was performed for data collection (temperature, heat flux, and spectral decomposition). The low average thermostat temperature of 50 K was used to obtain ballistic transport, with a temperature bias of 10 K. The thermostat coupling time was 50 fs.

To assess convergence, we divided each production trajectory into 2 consecutive blocks and verified that the integrated and spectral conductance were stable to within 5%. The reported $G(\omega)$ is the average over three independent trajectories initialized with different velocity seeds.

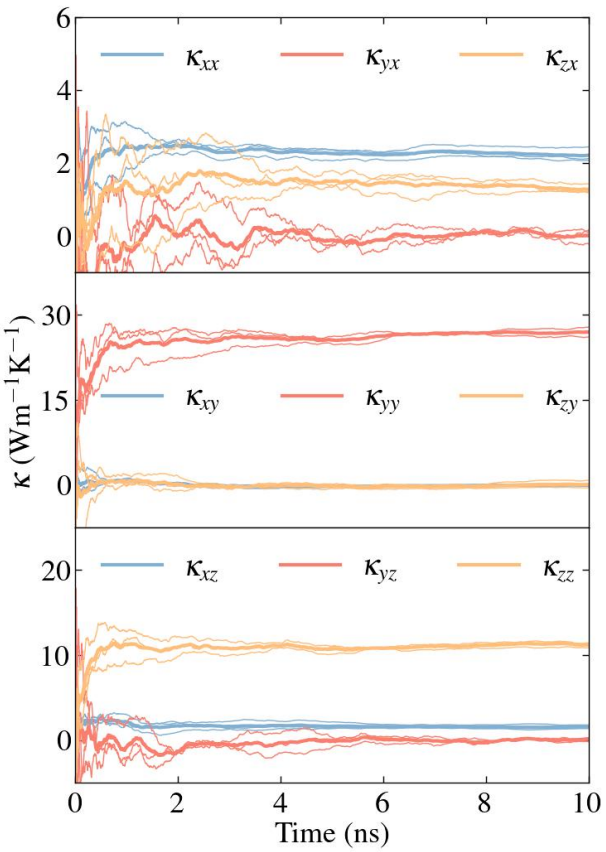

Figure S2. Full tensor calculation of Ta_2PdS_6 lattice thermal conductivity (LTC) at 300K.

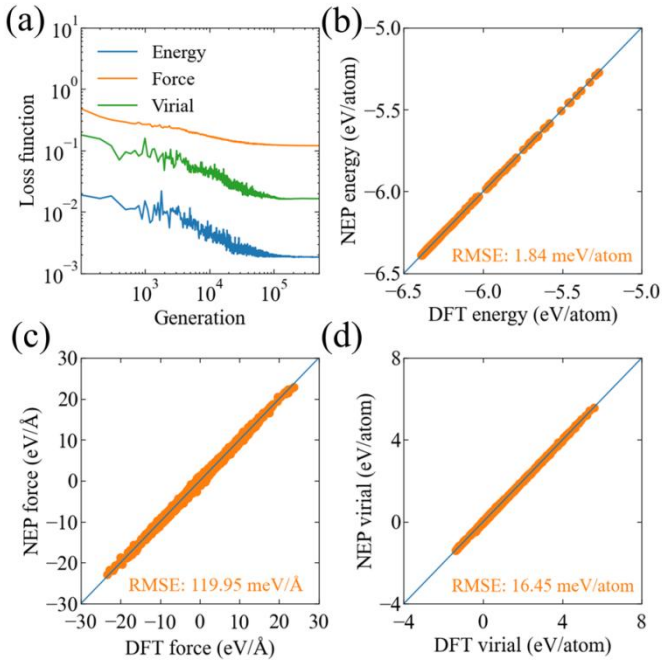

Figure S3. (a) Nb_2PdS_6 NEP model training iterative process of energy, force and viria; (b)-(d) Parity plot of energy, force and virial.

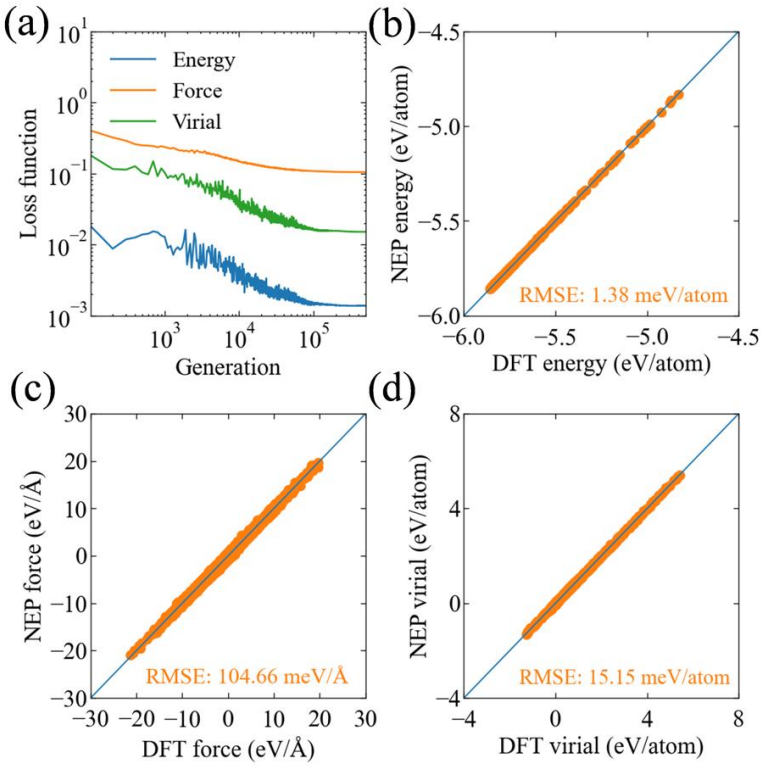

Figure S4. (a) Nb_2PdSe_6 NEP model training iterative process of energy, force and virial; (b)-(d) Parity plot of energy, force and virial.

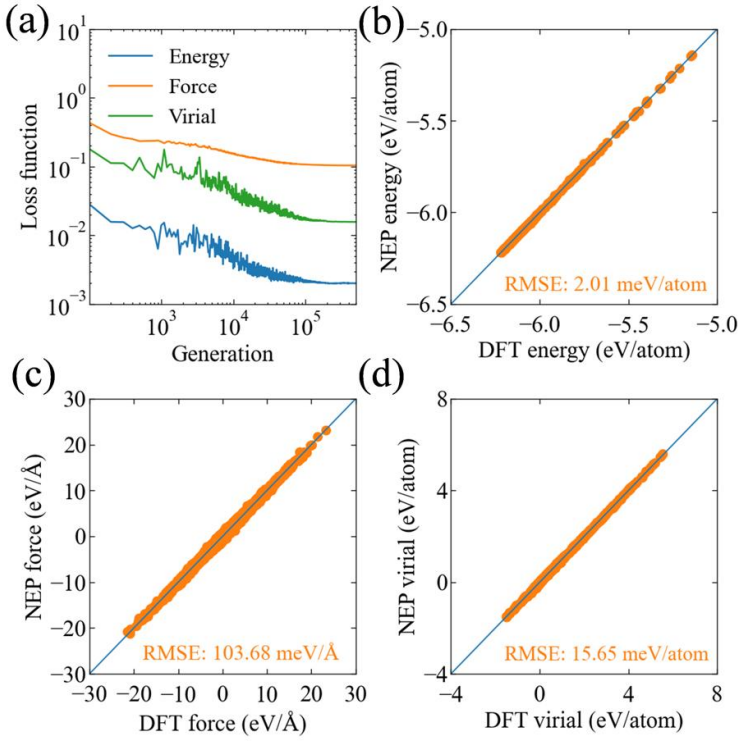

Figure S5. (a) Ta_2PdSe_6 NEP model training iterative process of energy, force and virial; (b)-(d) Parity plot of energy, force and virial.

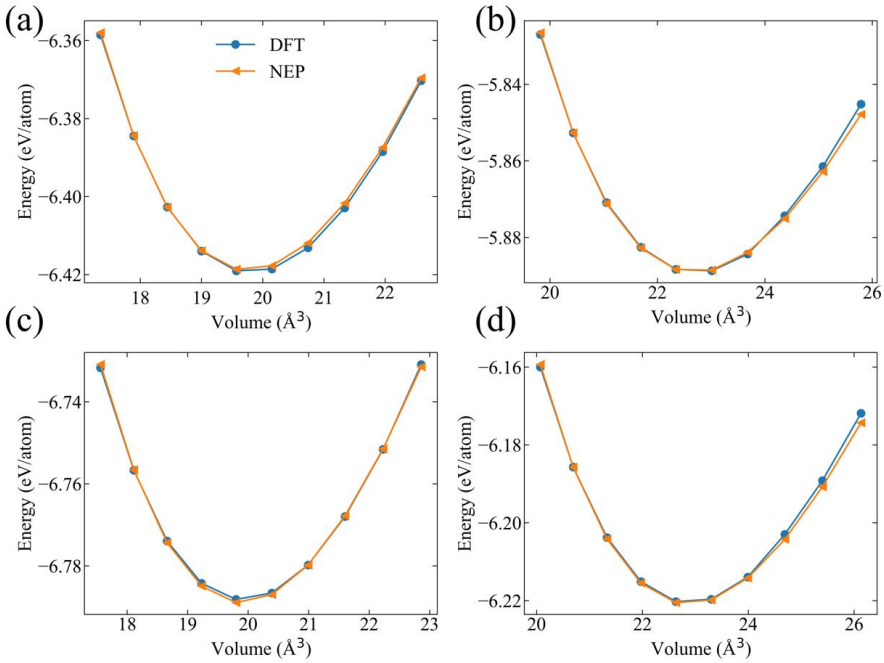

Figure S6. Predicted NEP and DFT-calculated energy-volume relationships for (a) Nb_2PdS_6; (b) Nb_2PdSe_6; (c) Ta_2PdS_6; (d) Ta_2PdSe_6.

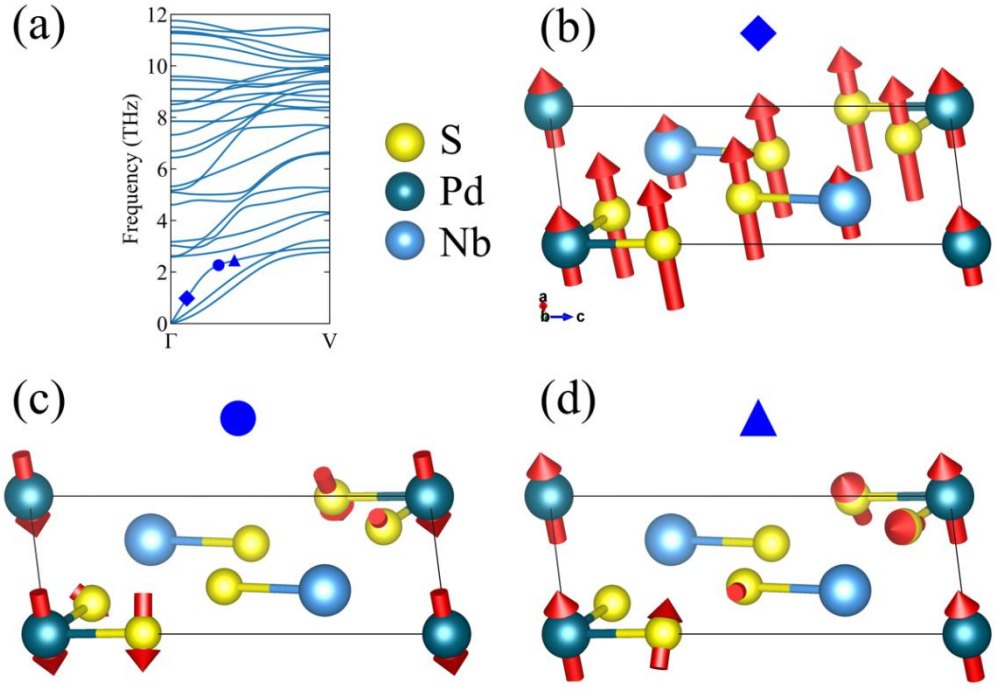

Figure S7. (a) Phonon dispersion curve of Nb_2PdS_6. Visualization of phonon vibration modes marked in the dispersion curve: (b) Diamond; (c) Circle; (d) Triangle.

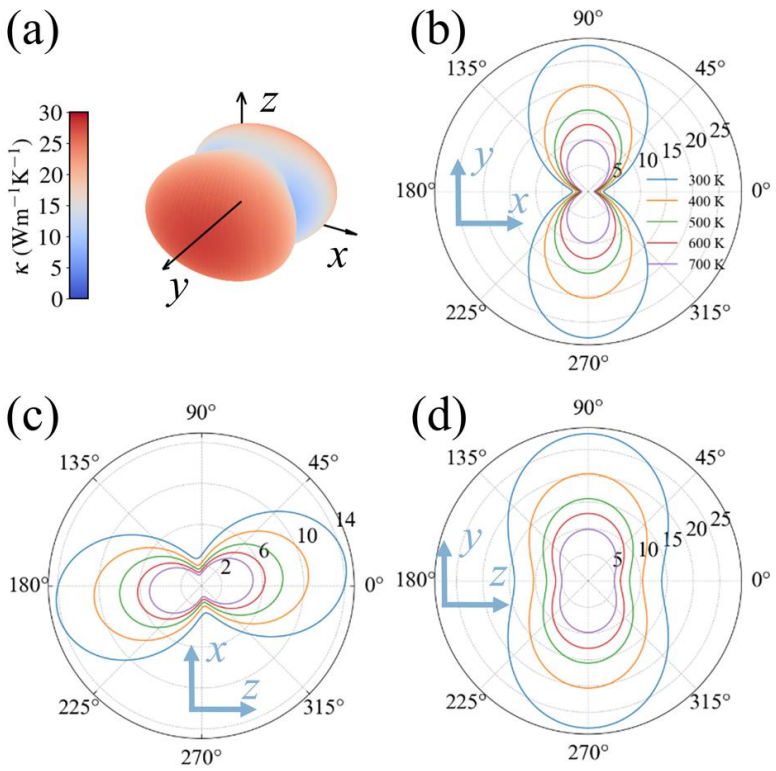

Figure S8. (a) Polar plot of LTC for Nb_2PdS_6 at 300K; (b)-(d)Two-dimensional projection maps of LTC on the crystal planes {001} (b), {010} (c), and {100} (d). The units for LTC are all $Wm^{-1}K^{-1}$.

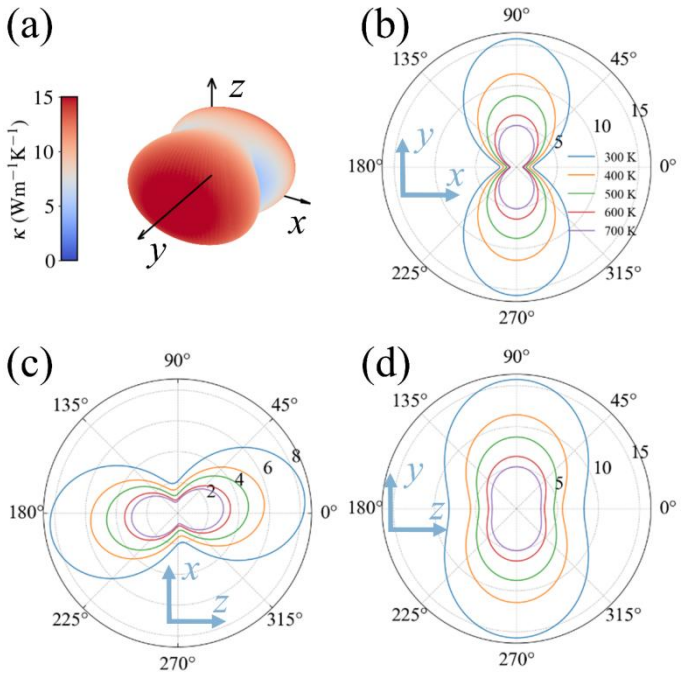

Figure S9. (a) Polar plot of LTC for Nb_2PdSe_6 at 300K. (b) - (d)Two-dimensional projection maps of LTC on the crystal planes {001} (b), {010} (c), and {100} (d). The units for LTC are all Wm^{-1} K^{-1}.

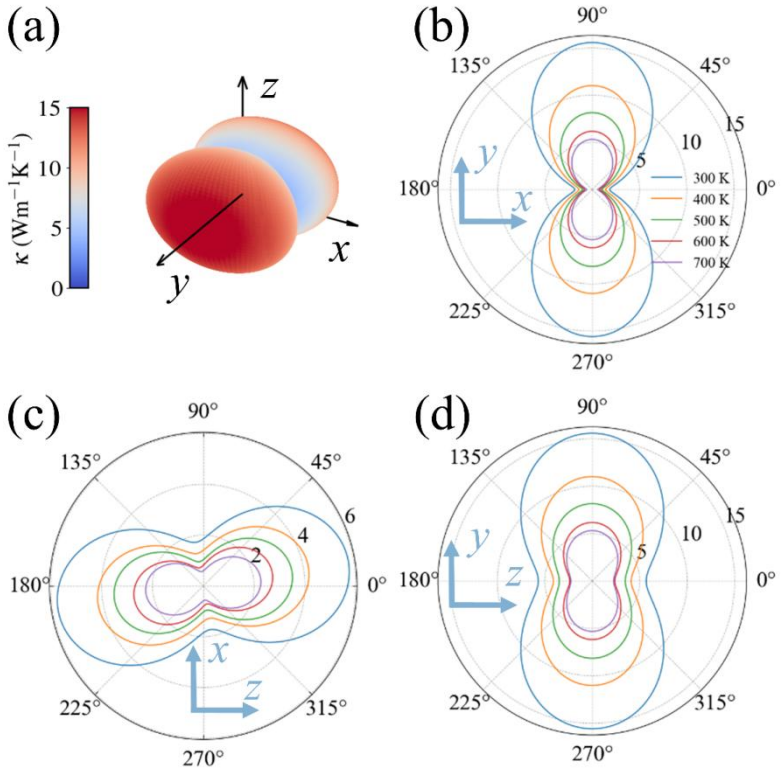

Figure S10. (a) Polar plot of LTC for Ta_2PdSe_6 at 300K. (b) - (d)Two-dimensional projection maps of LTC on the crystal planes {001} (b), {010} (c), and {100} (d). The units for LTC are all Wm^{-1} K^{-1}.

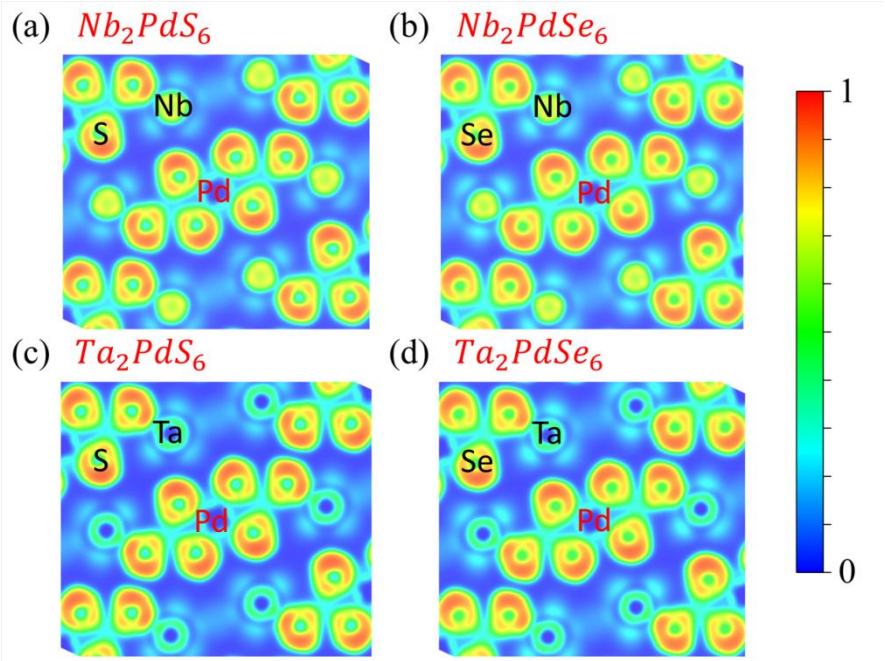

Figure S11. Distribution of the electron localization function (ELF) for bulk X_2PdY_6 (X=Nb, Ta; Y=S, Se) on the (010) plane. (a)Nb_2PdS_6, (b)Nb_2PdSe_6, (c)Ta_2PdS_6, and (d)Ta_2PdSe_6.

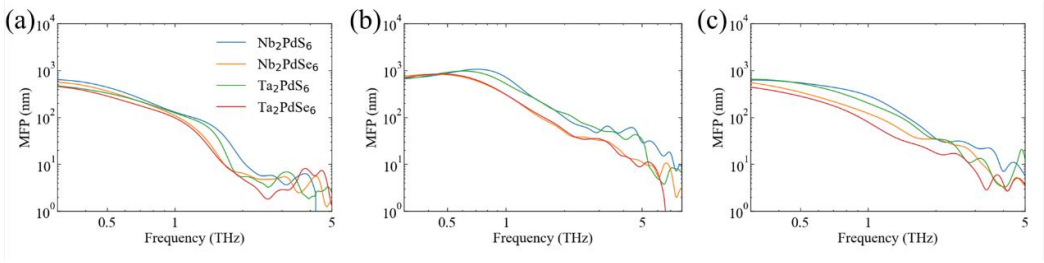

Figure S12. Phonon mean free path (MFP) of bulk X_2PdY_6 at 300K: (a) along the *x*-axis, (b) along the *y*-axis, and (c) along the *z*-axis.

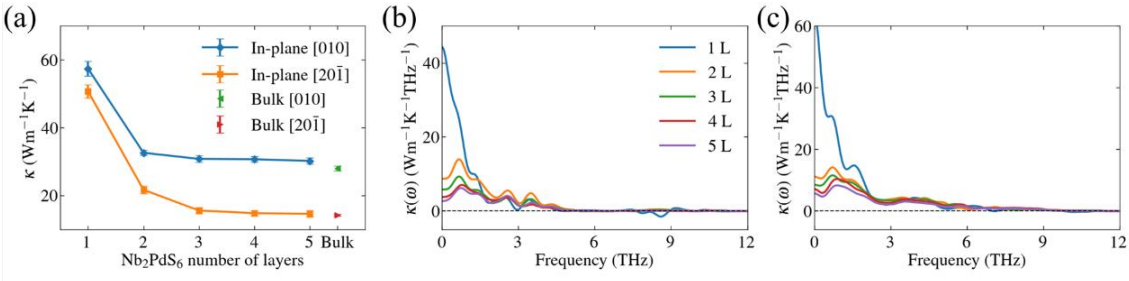

Figure S13. (a) The variation of Nb_2PdS_6 LTC with different layer numbers, with bulk LTC included for comparison; (b)-(c) Spectral decomposition of thermal conductivity along the in-plane [20$\bar{1}$] and [010] directions for 1-5 L.

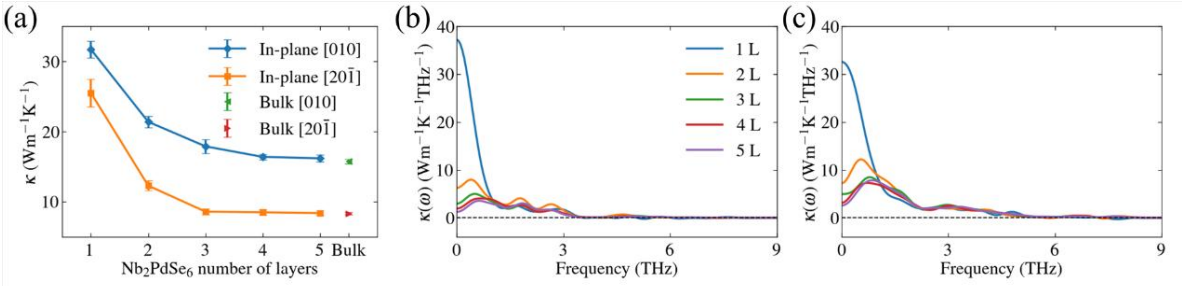

Figure S14. (a)The variation of Nb_2PdSe_6 LTC with different layer numbers, with bulk LTC included for comparison; (b)-(c) Spectral decomposition of thermal conductivity along the in-plane [20$\bar{1}$] and [010] directions for 1-5 L.

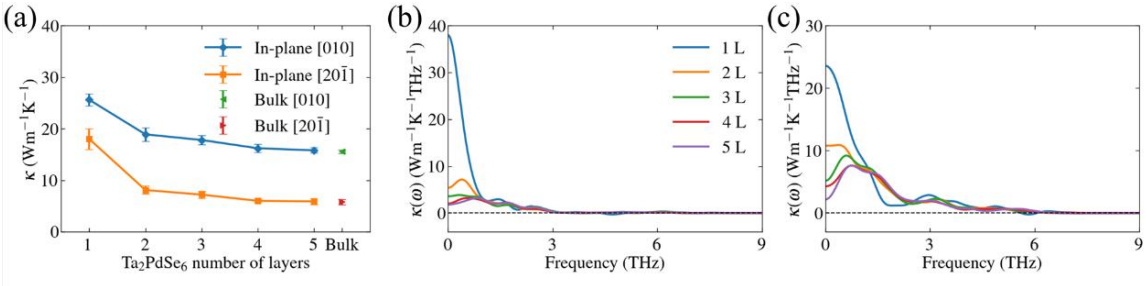

Figure S15. (a)The variation of Ta_2PdSe_6 LTC with different layer numbers, with bulk LTC included for comparison; (b)-(c) Spectral decomposition of thermal conductivity along the in-plane [20$\bar{1}$] and [010] directions for 1-5 L.

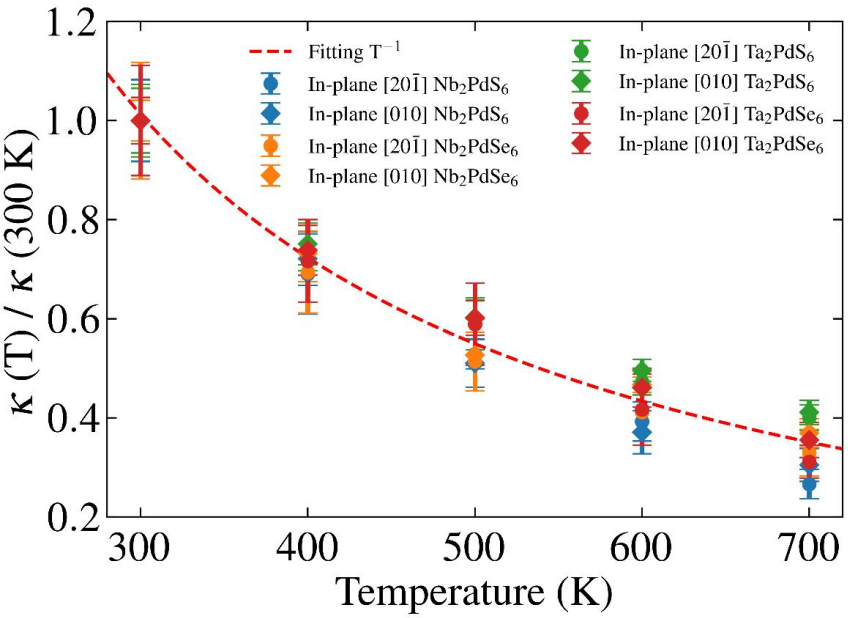

Figure S16. The reduced LTC of monolayer Nb_2PdS_6, Nb_2PdSe_6, Ta_2PdS_6, and Ta_2PdSe_6 along the in-plane [20 $\bar{1}$] and [010] crystal directions as a function of temperature. All LTC values are normalized by their respective values at 300 K.

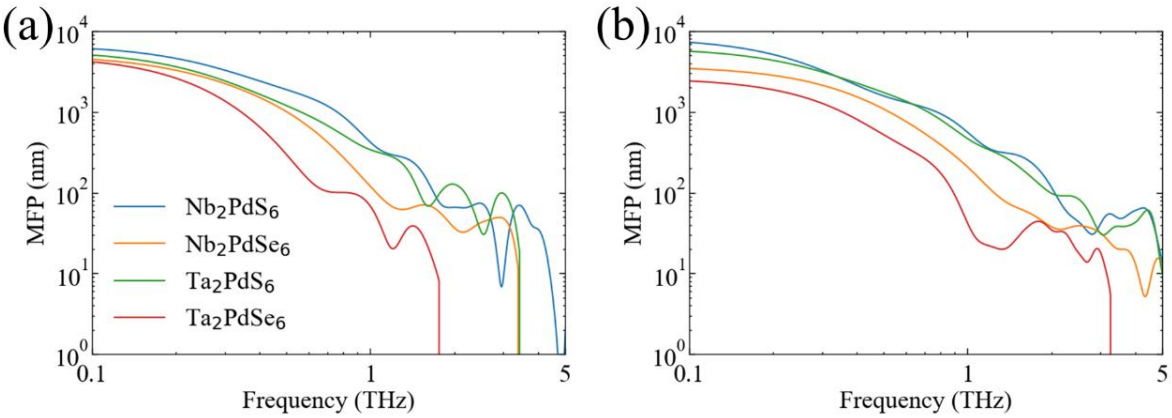

Figure S17. Phonon MFP of monolayer X_2PdY_6 at 300K: (a) along the *x*-axis and (b) along the *y*-axis.

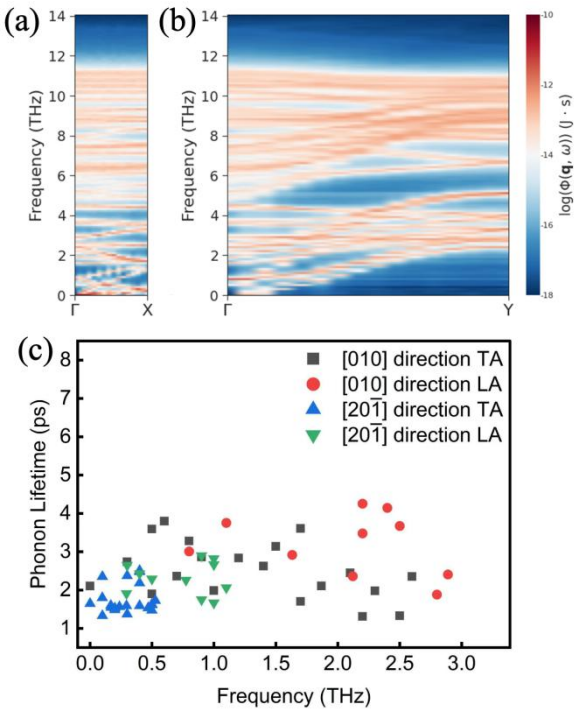

Figure S18. SED of monolayer Ta_2PdS_6 along the (a) [20$\bar{1}$] direction and (b) [010] direction. (c) phonon lifetimes of the resolved TA and LA modes along the [010] and [20$\bar{1}$] directions.

Because the 18-atom monolayer unit cell gives rise to 54 phonon branches, substantial overlap occurs among the SED peaks. Only clearly resolved LA and TA peaks were fitted using Lorentzian functions; therefore, the extracted lifetimes are used for qualitative directional comparison rather than exhaustive mode-by-mode quantification.

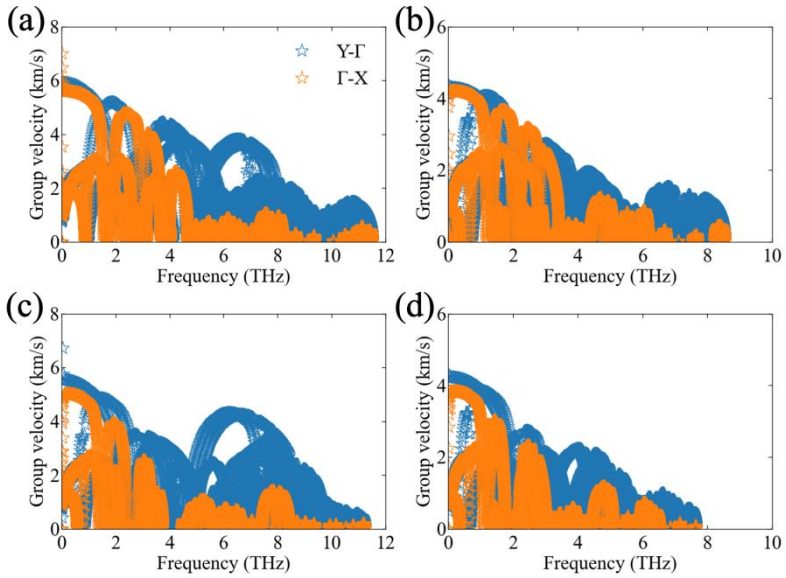

Figure S19. Phonon group velocity of monolayer structures along the [20$\bar{1}$] direction (X) and [010] direction (Y) calculated based on NEP for (a) Nb_2PdS_6; (b) Nb_2PdSe_6; (c) Ta_2PdS_6; (d) Ta_2PdSe_6.

Table S1. The composition of the training dataset. All the four compounds use training datasets with the same composition.

Condition 1	Condition 2	Number of structures	Ratio
Bulk AIMD	100 K	10	2.5%
	300 K	10	2.5%
	500 K	10	2.5%
	800 K	10	2.5%
	1200 K	10	2.5%
	1600 K	10	2.5%
Bulk deformation + random displacement	±5% and 0.1 Å	10	2.5%
	±5% and 0.3 Å	10	2.5%
	±3% and 0.1 Å	10	2.5%
	±3% and 0.3 Å	10	2.5%
	±2% and 0.1 Å	10	2.5%
	±2% and 0.3 Å	10	2.5%
	±1% and 0.1 Å	10	2.5%
	±1% and 0.3 Å	10	2.5%
	±0.5% and 0.1 Å	10	2.5%
	±0.5% and 0.3 Å	10	2.5%
	0% and 0.1 Å	5	1.25%
	0% and 0.3 Å	5	1.25%
2D structure AIMD	100 K	20	5%
	300 K	20	5%
	600 K	20	5%
	1000 K	20	5%
2D structure deformation + random displacement	±2% and 0.1 Å	10	2.5%
	±2% and 0.3 Å	10	2.5%
	±1% and 0.1 Å	10	2.5%
	±1% and 0.3 Å	10	2.5%
	0% and 0.1 Å	5	1.25%
	0% and 0.3 Å	5	1.25%
Active learning		100	25%
Total		400	100%

Table S2. LTC tensor at 300 K.

$\kappa_{Nb_2PdS_6} = \begin{pmatrix} 2.98 & 0.0 & 1.80 \\ 0.0 & 27.99 & 0.0 \\ 1.80 & 0.0 & 13.99 \end{pmatrix}$	$\kappa_{Nb_2PdSe_6} = \begin{pmatrix} 2.06 & 0.0 & 0.90 \\ 0.0 & 15.75 & 0.0 \\ 0.90 & 0.0 & 8.22 \end{pmatrix}$
$\kappa_{Ta_2PdS_6} = \begin{pmatrix} 2.16 & 0.0 & 1.42 \\ 0.0 & 27.6 & 0.0 \\ 1.42 & 0.0 & 10.74 \end{pmatrix}$	$\kappa_{Ta_2PdSe_6} = \begin{pmatrix} 1.85 & 0.0 & 0.70 \\ 0.0 & 15.58 & 0.0 \\ 0.70 & 0.0 & 5.68 \end{pmatrix}$

Table S3. Comparison of κ_{xx} with $\kappa_{[102]}$ and of κ_{zz} with $\kappa_{[20\bar{1}]}$. LTC is reported in $Wm^{-1} K^{-1}$.

Materials	κ_{xx}	$\kappa_{[102]}$	Relative deviation (%)	κ_{zz}	$\kappa_{[20\bar{1}]}$	Relative deviation (%)
Nb_2PdS_6	2.98	2.70	10.4%	13.99	14.27	2.0%
Nb_2PdSe_6	2.06	1.94	6.2%	8.22	8.34	1.4%
Ta_2PdS_6	2.16	1.93	11.9%	10.70	10.97	2.5%
Ta_2PdSe_6	1.85	1.73	6.9%	5.69	5.80	1.9%